

PCCP

Accepted Manuscript



This is an *Accepted Manuscript*, which has been through the Royal Society of Chemistry peer review process and has been accepted for publication.

Accepted Manuscripts are published online shortly after acceptance, before technical editing, formatting and proof reading. Using this free service, authors can make their results available to the community, in citable form, before we publish the edited article. We will replace this *Accepted Manuscript* with the edited and formatted *Advance Article* as soon as it is available.

You can find more information about *Accepted Manuscripts* in the [Information for Authors](#).

Please note that technical editing may introduce minor changes to the text and/or graphics, which may alter content. The journal's standard [Terms & Conditions](#) and the [Ethical guidelines](#) still apply. In no event shall the Royal Society of Chemistry be held responsible for any errors or omissions in this *Accepted Manuscript* or any consequences arising from the use of any information it contains.

ARTICLE

Structure of $\text{H}_2\text{Ti}_3\text{O}_7$ and its evolution during Sodium insertion as anode for Na Ion Batteries

Cite this: DOI: 10.1039/x0xx00000x

Aitor Eguía-Barrio^{a,b}, Elizabeth Castillo-Martínez^{a*}, Maider Zarrabeitia^a, Miguel A. Muñoz-Márquez^a, Montse Casas-Cabanas^a, Teófilo Rojo^{a,b*}

Received 00th January 2013,

Accepted 00th January 2013

DOI: 10.1039/x0xx00000x

www.rsc.org/

$\text{H}_2\text{Ti}_3\text{O}_7$ was prepared as a single phase by ionic exchange from $\text{Na}_2\text{Ti}_3\text{O}_7$. The complete ionic exchange was confirmed by ^1H and ^{23}Na solid state NMR. The atomic positions of $\text{H}_2\text{Ti}_3\text{O}_7$ were obtained from the Rietveld refinement of powder X-ray diffraction and neutron diffraction experimental data, the latter collected at two different wavelengths to precisely determine the hydrogen atomic positions in the structure. All H^+ cations are hydrogen bonded to two adjacent $[\text{Ti}_3\text{O}_7]^{2-}$ layers leading to the gliding of the layers and lattice centring with respect to the parent $\text{Na}_2\text{Ti}_3\text{O}_7$. In contrast with a previous report where protons were located in two different positions of $\text{H}_2\text{Ti}_3\text{O}_7$, 3 types of proton positions were found. Two of the three types of protons are bonded to the only oxygen linked to a single titanium atom forming an H-O-H angle close to that of the water molecule. $\text{H}_2\text{Ti}_3\text{O}_7$ is able to electrochemically insert Na^+ . The electrochemical insertion of sodium in $\text{H}_2\text{Ti}_3\text{O}_7$ starts with a solid solution regime of the C-centred phase. Then, between 0.6 and 1.2 inserted Na^+ the reaction proceeds through a two phase reaction and a plateau at 1.3 V vs Na^+/Na is observed in the voltage-composition curve. The second phase resembles the primitive $\text{Na}_2\text{Ti}_3\text{O}_7$ cell as detected by *in-situ* XRD. Upon oxidation, from 0.9 to 2.2V, the PXRD pattern remains mostly unchanged probably due to H^+ removal instead of Na^+ , with the capacity quickly fading upon cycling. Conditioning $\text{H}_2\text{Ti}_3\text{O}_7$ for two cycles at 0.9-2.2 V before cycling in the 0.05-1.6 V range yields similar specific capacity and better retention than the original $\text{Na}_2\text{Ti}_3\text{O}_7$ in the same voltage range.

1. Introduction

Nowadays there is a need to improve energy storage systems in order to fully utilize renewable and clean energy sources which suffer from variability in time and in space. For mobile applications the field of lithium ion batteries has undergone tremendous development due to their high energy density.¹ However, lithium reserves are located in politically sensitive areas, while sodium is spread worldwide and it can be obtained at a much lower cost.² Therefore, research on sodium ion batteries is being developed for stationary storage applications in which the weight of the device is not a key aspect. In addition the possible use of aluminium as anode current collector in sodium ion batteries instead of copper can counteract the energy density penalty resulting from moving from lithium to sodium ion batteries.

More challenging than in lithium ion batteries, finding an appropriate anode that fulfills all requirements remains elusive. During the last year many materials were proposed as anodes for sodium ion batteries.³ The most promising results in terms of capacity are shown by phosphorus-carbon composites that deliver more than 1500 mAh/g,^{4,5} however it requires special handling conditions and its reduction product Na_3P can lead to dangerous phosphine, PH_3 . Sn/C^6 or Sb/C^7 composites have also shown good performance with capacities close to 600 mAh/g sustained for more than 100 cycles, but they are more expensive due to its relatively

medium abundance. The use of organic electrodes,⁸ polymeric,⁹ hard carbons,¹⁰ or sodium titanates,¹¹ which deliver moderate capacities up to 300 mAh/g still seem the safest and most cost effective path in the search of anode materials.

Sodium titanates can be prepared through simple solid state routes from relatively cheap raw materials.¹² Amongst sodium titanates the zig-zag layered oxide $\text{Na}_2\text{Ti}_3\text{O}_7$ exhibits the lowest insertion voltage reported for Na-ion batteries, being capable of intercalating/deintercalating two sodium ions per formula unit at average voltages as low as 0.3 V vs Na^+/Na .¹¹ The material presents however, a continuous capacity fading upon cycling that has been reported to be partially alleviated by substituting Na_2CO_3 by NaOH during synthesis,¹³ although the exact origin for this improvement remains unclear. Carbon coating has also shown to be helpful in increasing the coulombic efficiency.¹⁴ Few years ago it was shown that lithium can also be inserted into $\text{Na}_2\text{Ti}_3\text{O}_7$ with an initial capacity of only 50 mAh/g in the voltage range between 1.0-1.6 V.¹⁵ In the same study Chiba *et al.* exchanged sodium by lithium and found that the isostructural phase $\text{Li}_2\text{Ti}_3\text{O}_7$ is able to deliver a capacity as high as 140 mAh/g when cycled vs Li^+/Li at an average voltage of 1.5 V, despite the capacity fades almost 50% after 10

cycles.¹⁵ The structurally related $\text{H}_2\text{Ti}_3\text{O}_7$ can also be prepared through ionic exchange in acidic aqueous media.¹⁶

In fact, in 2011, Akimoto *et al.* reported the electrochemical performance of $\text{H}_2\text{Ti}_3\text{O}_7$ vs lithium, as well as that of two of its dehydrated phases, $\text{H}_2\text{Ti}_6\text{O}_{13}$ and $\text{H}_2\text{Ti}_{12}\text{O}_{25}$, and found capacities close to 200 mAh/g for the latter two phases and close to 175 mAh/g for $\text{H}_2\text{Ti}_3\text{O}_7$.¹⁷ $\text{H}_2\text{Ti}_3\text{O}_7$ has the same individual $[\text{TiO}_6]_n$ zig-zag layers than $\text{Na}_2\text{Ti}_3\text{O}_7$ although, instead of being stacked in a primitive lattice, they are C-centered because of a relative displacement of $b/2$, yielding a doubling of the unit cell (Figure 1).¹⁸

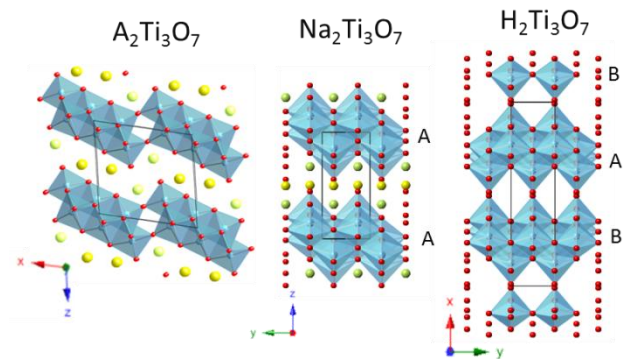


Figure 1. View along the z axis of $\text{Na}_2\text{Ti}_3\text{O}_7$ ($P2_1/m$) and view along the x axis of $\text{Na}_2\text{Ti}_3\text{O}_7$ ($P2_1/m$) and $\text{H}_2\text{Ti}_3\text{O}_7$ ($C2/m$) showing the shift of layers along the b axis.

Two different types of protons were recently determined from refinement of neutron diffraction data, nevertheless an unexpectedly large value of Ti valence was calculated by the BVS method.¹⁹

Encouraged by the much higher capacity observed in $\text{H}_2\text{Ti}_3\text{O}_7$ with respect to $\text{Na}_2\text{Ti}_3\text{O}_7$ in Li-ion batteries herein we study the electrochemical performance of this phase for Na-ion batteries. Additionally we had independently decided to complete the structure determination of $\text{H}_2\text{Ti}_3\text{O}_7$, which happens to show some differences with that recently reported.

2. Experimental

Sample preparation. The sodium titanate $\text{Na}_2\text{Ti}_3\text{O}_7$ was prepared by mixing 5% excess $\text{Na}_2\text{CO}_3 \cdot \text{H}_2\text{O}$ with TiO_2 anatase (Sigma) in the ratio 1:3, and heating up to 800°C for 36 hours with two intermediate grindings. To prepare the protonated phase $\text{H}_2\text{Ti}_3\text{O}_7$,¹⁶ an ionic exchange in a “ten-fold” excess of 0.1M HNO_3 refluxing at 60°C for 6 h was carried out yielding a single phase according to powder X-ray diffraction (PXRD) as well as ^{23}Na and ^1H solid state nuclear magnetic resonance (ssNMR).

Materials Characterization. Synthesized powdered samples were studied by conventional PXRD on a Bruker Advance D8 instrument with copper radiation ($\text{Cu K}\alpha$, $\lambda=1.5418 \text{ \AA}$). PXRD data for structure refinement were collected in the 2θ X-ray range from 5° to 80° with a step time of 0.14°/minute. Neutron diffraction data were collected at the D1B instrument (ILL, France) at room temperature and using two different wavelengths ($\lambda=1.28 \text{ \AA}$ and $\lambda=2.52 \text{ \AA}$) over the 2θ range 0.77–128.67°. Rietveld refinements were done with the FullProf program.²⁰ The peak shapes were modeled with a Thompson-Cox-Hastings pseudo-Voigt function. Scale factors, zero point,

unit cell constants, atomic positions, temperature factors and atomic occupancies were refined simultaneously.

Combined PXRD and NPD Rietveld refinements were also carried out for $\text{H}_2\text{Ti}_3\text{O}_7$, starting with the previously reported structural model without including any protons between the $[\text{Ti}_3\text{O}_7]^{2-}_n$ layers.¹⁸ The H^+ cations were located by nuclear scattering density Fourier difference maps from Rietveld refinement of neutron diffraction data at $\lambda=2.52 \text{ \AA}$ with the GFourier program included in the FullProf package.

^1H and ^{23}Na solid state NMR data were collected on a Bruker 500 MHz spectrometer, at an operating frequency of 500 MHz and 132 MHz for ^1H and ^{23}Na respectively. 1.3 mm rotors were spun at the magic angle at a spinning rate of 50 kHz. A rotor synchronized Hahn echo ($90^\circ\text{-}\tau\text{-}180^\circ\text{-}\tau\text{-acq.}$) sequence was used with a 90° pulse of 2.75 μs (^1H) and 1.5 μs (^{23}Na) and a delay of 40 s for both nuclei; 160 scans were collected per ^1H spectra. ^1H spectra are referenced to a secondary reference, H_2O (4.8 ppm). 1440 scans were collected per ^{23}Na spectrum, the spectra being referenced to a 1M NaCl aqueous solution. To make a quantitative estimation of the amount of ^{23}Na remaining after exchange the spectra were normalized with respect to the sample weight and number of scans. Fitting and integration of the spectra was done with DMFit.²¹

Electrochemical Characterization. The electrochemical performance was tested in CR2032 coin type cells vs. sodium metal, using glass fibre (Whatman GF B 55) as separator and 1M NaClO_4 in Ethylene Carbonate-Dimethyl Carbonate mixture 1:1 (EC:DMC) as electrolyte. Electrodes were prepared by mixing approximately 80% active material with 10% carbon Super C-65 (Timcal) and 10% PvdF in NMP. The mixed slurry was casted on battery grade aluminium foil with the Dr. Blade technique. The laminates were vacuum dried for 12 h at 80°C prior to punching and pressing the electrodes. After additional vacuum drying for 12 h at 80°C, electrodes were inserted in an argon filled glove box and batteries were assembled. The typical electrode loading were 1.8–5.4 mg/cm^2 . For in-situ PXRD, a homemade cell design based on a 1-inch Swagelok cell was used and the working electrodes were used in powder form with 65% active material and 35% carbon Super C-65 that were hand mixed in an agate mortar and dried at 80°C for 12 hours prior to cell assembly with 2 glass fibre Whatmann separators and a metallic sodium foil as counter electrode. The same electrolyte 1M NaClO_4 in EC:DMC was used.

3. Results and discussion

Structural Characterization. All prepared samples were white powders. The plot of the Rietveld refinement of the PXRD data is shown in Figure 2. It can be seen that pure phases were obtained for $\text{Na}_2\text{Ti}_3\text{O}_7$ and $\text{H}_2\text{Ti}_3\text{O}_7$. Lattice parameters are in agreement with those reported in the literature (see table 1).^{12, 18}

The structural study of the protonated phase was completed with the location of the protons through neutron diffraction measurements at D1B (ILL). First, combined Rietveld refinement of X-rays and the two neutron diffraction patterns collected at two different wavelengths ($\lambda=1.28 \text{ \AA}$ and $\lambda=2.52 \text{ \AA}$) was done without hydrogen atoms. The differential Fourier map along the ac plane at the $y=0.5$ section (Figure 3a) shows the location of three protons H1, H2 and H3 at $2a$, $4i$ and $2c$ Wyckoff positions respectively, where residual negative scattering appeared. Introducing the three H^+ in the structure for the combined Rietveld refinement of X-rays and the two

neutron diffraction patterns resulted in a good fit, (Figure 3b, Figure S2 and Table S1) and yielded the proton positions as depicted in Figure 3c which can be considered as a good first approximation.

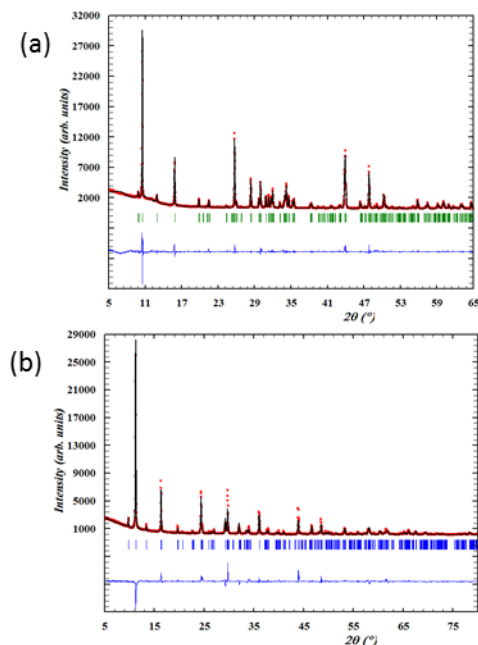


Figure 2. Observed (red dots), calculated (solid line), and difference (bottom) patterns for the Rietveld analysis from the powder X-ray diffraction data of $\text{H}_2\text{Ti}_3\text{O}_7$ (a) and $\text{Na}_2\text{Ti}_3\text{O}_7$ (b). Short vertical lines below the profile

Material	<i>a</i>	<i>b</i>	<i>c</i>	β
$\text{Na}_2\text{Ti}_3\text{O}_7$	9.124454(3) Å	3.800515(2) Å	8.561921(3) Å	101.5946(1) $^\circ$
$\text{H}_2\text{Ti}_3\text{O}_7$	16.0243(1) Å	3.74973(5) Å	9.1888(2) Å	101.4384(2) $^\circ$

indicate the peak positions of all the possible Bragg reflections.

Table 1. Lattice parameters of parent $\text{Na}_2\text{Ti}_3\text{O}_7$ ($P2_1/m$) and the studied material $\text{H}_2\text{Ti}_3\text{O}_7$ ($C2/m$). A doubling of the unit cell is obtained along *c* (along *a* for the protonated titanate) due to the shift of $[\text{Ti}_3\text{O}_7]^{2-}$ layers during ionic exchange.

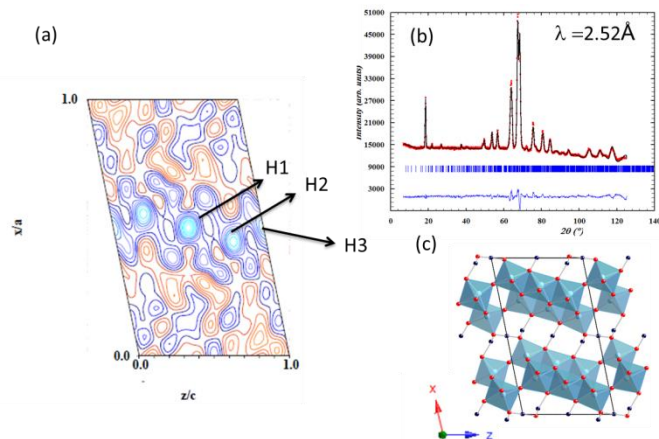


Figure 3. Proton location from neutron diffraction (a) Differential Fourier map at *ac* plane in the $y=0.5$ section. Blue lines represent negative intensity due to the negative proton scattering length for neutron radiation. (b) Rietveld refined neutron diffraction pattern collected at $\lambda=2.52$ Å from the combined refinement of X-Ray Diffraction and 2 different wavelengths

neutron diffraction data (c) view of the resolved structure of $\text{H}_2\text{Ti}_3\text{O}_7$ along the *y* axis containing the three different protons. Black spheres correspond to hydrogen atoms, red spheres to oxygen atoms and titanium atoms are in the centre of turquoise octahedra.

Since the thermal displacement parameters (B_{iso} , Table S2) achieved for the hydrogen atoms are quite large, and comparable to those reported by *Kataoka et al.* (~ 5 Å 2), we selected the higher resolution neutron diffraction pattern ($\lambda=1.28$ Å) to better refine hydrogen positions and thermal displacements and explore possible splittings. First we introduced microstructural parameters with strain broadening in the refinement, which significantly improved the agreement factors (Table S3) although the thermal displacement factor remained large. By independent refinement of the thermal displacement factor of the three H atoms it was clear that H1 and H3 showed much larger values. Splitting of H1 into 2 positions as *Kataoka et al.* did¹⁹ led to equivalent atoms 1 Å apart. Since both positions cannot be simultaneously occupied, the site population was set to a half of its value (Figure 4b). Moreover anisotropic thermal parameters were considered for both H1 and H3 while H2 remained unsplit with an isotropic thermal displacement of ~ 2.0 Å 2 . The refinement of these parameters provides more precise $-\text{O}-\text{H}$ distances. However other atomic positions, interatomic distances and angles remain largely unchanged (comparing table S2 and S4).

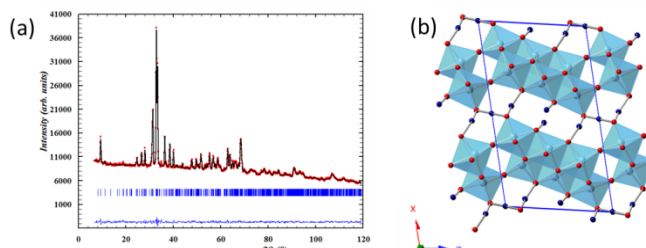


Figure 4. Plot of the Rietveld refined neutron diffraction pattern collected at $\lambda=1.28$ Å with anisotropic strain model, H1 splitting and H1, H3 with anisotropic thermal displacement parameters (a). View along the *y* axis of the resulting structure of $\text{H}_2\text{Ti}_3\text{O}_7$ (b).

It is interesting to observe that the H^+ cations are located in the same (0 0 0) planes as the neighboring oxygen atoms and not in the prismatic holes between oxygen layers, which is the position of sodium atoms in $\text{Na}_2\text{Ti}_3\text{O}_7$. This different coordinating preference of H^+ and Na^+ might be the reason for the change of symmetry from the sodiated to the protonated titanate. Looking at the proton environments (Figure 4b) it is seen that all H^+ are hydrogen bonded to two oxygen atoms from different layers. The splitted proton located close to the center of the unit cell (H1) is in a Wyckoff position 4i with occupancy of 0.25 (half of the total site population), with O3-H1 distances of 1.96 Å and 0.91 Å. The second proton (H2) is fully occupied, and is covalently bonded to O4, with a bond of 0.99 Å and a longer hydrogen bond of 1.64 Å to the opposite oxygen (O2-H2-O4 angle of 170 $^\circ$). On the other hand the third proton (H3) in the wickoff position 2c is also totally occupied with H3-O4 distances of 1.32 Å.

All these short interlayer O-H-O bonds (Table S3) are likely the driving force for the structural transition from the primitive unit cell of the sodium titanate to the C-centered unit cell of the protonated analogue.

It is worth to mention that the H2-O4-H3 angle, 102° , is very close to that found in water, 104.5° as well as the 0.99 \AA for the H2-O4 distance. This suggests that H2-O4-H3 might be the water molecule leaving $\text{H}_2\text{Ti}_3\text{O}_7$ when it is heated and $\text{H}_2\text{Ti}_{12}\text{O}_{25}$ and $\text{H}_2\text{Ti}_6\text{O}_{13}$ are obtained.¹⁷ The calculated bond valence sums (BVS) of Titanium and Hydrogen ions were calculated with the same parameters than Kataoka et al. The calculated values were: Ti1, 4.21(8); Ti2, 4.18(9); Ti3, 4.11(7); H1, 0.93(5); H2, 0.97(2); H3, 0.90(1), which are in agreement with the formal valence of Ti^{4+} and H^+ .

Moreover, two signals can be resolved in the ^1H -NMR spectrum of $\text{H}_2\text{Ti}_3\text{O}_7$ (Figure 5) at 11 and 13 ppm. These two signals can be correlated with two different $-\text{OH}$ stretchings appearing in the infrared spectrum at 2920 cm^{-1} and 3190 cm^{-1} respectively (Figure S1). The higher frequency of absorption in the infrared, 3190 cm^{-1} , corresponds to the shorter O-H distance which is likely to correspond to the less shifted signal of the ^1H NMR spectrum. Concomitant to the existence of the two ^1H signals there is a negligible ^{23}Na signal in the NMR spectrum with a small peak at about 7.2 ppm which can be assigned to less than 1% residual sodium as calculated to remain in $\text{H}_2\text{Ti}_3\text{O}_7$ from the quantitative integration of the ^{23}Na -NMR signal of $\text{H}_2\text{Ti}_3\text{O}_7$ and $\text{Na}_2\text{Ti}_3\text{O}_7$. The narrowness of the peak might be due to very mobile residual surface sodium ions. Therefore, bulk exchange of Na^+ by H^+ is confirmed.

The relative integrated intensities of the two ^1H -NMR signals are 25% and 75% respectively, which would be in agreement with the fact that H1 has an occupancy of 0.25 whereas the two protons bonded to O4 (H2 and H3 with occupancies of 0.5 and 0.25 respectively) have overlapping chemical shift in the ^1H -NMR spectra. The possible splitting observed for H1 would agree with the highest proton mobility and the narrowest ^1H -NMR signal.

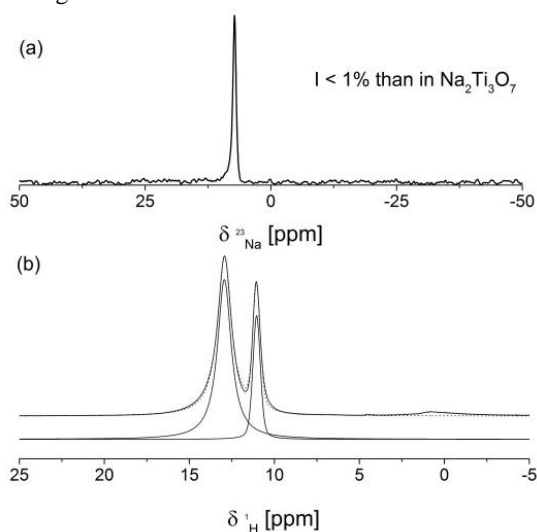


Figure 5. Magic Angle Spinning ($\nu=50\text{kHz}$) solid-state NMR spectra of $\text{H}_2\text{Ti}_3\text{O}_7$ (a) ^{23}Na and (b) ^1H .

Moreover it can be seen that ^1H -NMR spectra of $\text{H}_2\text{Ti}_3\text{O}_7$ was collected at very high spinning rates (50 kHz) which yields a much higher resolution spectra than the one previously reported

(12 kHz)¹⁷. This allowed to deconvolute the signals and integrate them, yielding a ratio of 1:3 which supports the structural model of 3 protons with total unit cell occupancies of 0.25 (H1), 0.5 (H2) and 0.25 (H3) as described in this paper.

The chemical shift of these two H^+ signals is larger than the values of 5 and 9 ppm reported for the tunnel like ramsdellite type allotrope $\text{H}_2\text{Ti}_3\text{O}_7$ ²² or the only signal appearing at 10 ppm for the unique type of H^+ in $\text{H}_2\text{Ti}_6\text{O}_{13}$.²³ This is indicative of a higher H^+ acidity in the layered $\text{H}_2\text{Ti}_3\text{O}_7$, whose most acidic protons should be those nearby the oxygen atom which is coordinated to only one titanium atom. This fact has not been observed neither in the ramsdellite phase nor the $\text{H}_2\text{Ti}_6\text{O}_{13}$ tunnel structure.

We should mention that there are several differences between our model and that recently reported by Kataoka et al.¹⁹ Their neutron diffraction study allowed them to locate only two of the three type of protons that we have located, which are almost at the same positions. However in their model, splitting H1 was not accompanied by a splitting of occupancies which results in two different protons equally abundant with very short H1-H1 interatomic distances. The reason for not observing the third proton could be due to the fact that they used a shorter wavelength, $\lambda=1.8 \text{ \AA}$ vs $\lambda=2.52 \text{ \AA}$ for one of our datasets, which made it less sensitive to the low angle reflections. In order to test the validity of the reported structure, we have attempted to refine our data with their model achieving poorer agreement (Table S 5).

Moreover the integration of the ^1H -NMR data fully supports the existence of 3 different proton sites two of them contributing to the same signal rather than two equally abundant protons.

Electrochemical characterization. Due to the structural similarities with $\text{Na}_2\text{Ti}_3\text{O}_7$, which inserts sodium at 0.3 V vs Na^+/Na , a low voltage for the insertion of sodium ions could be expected. This might be slightly increased due to the lower electropositivity of H^+ with respect to Na^+ , however a plateau corresponding to the insertion of one Na/f.u. is already observed at voltages as high as 1.3 V (Figure 6), which is much higher than expected, and similar to other titanium oxides.^{15,24} The profiles in different voltage ranges (high 0.9-3.0 V, medium 0.5-3.0 V and low 0.05-2.2 V) of $\text{H}_2\text{Ti}_3\text{O}_7$ vs. Na^+/Na for galvanostatic discharges at C/10 are shown in Figure 6. When $\text{H}_2\text{Ti}_3\text{O}_7$ is cycled down to 0.5 V or 0.005 V additional capacities are delivered, but without the corresponding reversibility in the charge capacity.

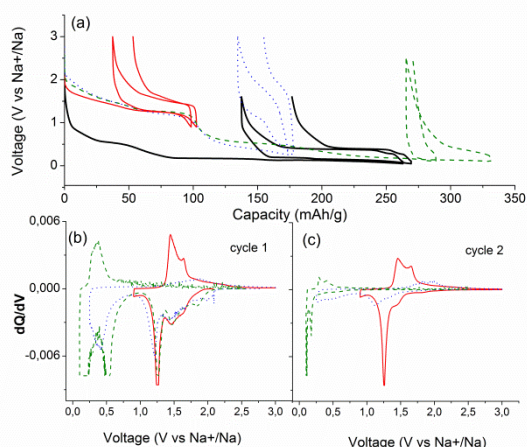


Figure 6. Electrochemical performance of $\text{H}_2\text{Ti}_3\text{O}_7$ vs Na^+/Na . (a) First and second cycle voltage vs capacity discharge profiles for $\text{H}_2\text{Ti}_3\text{O}_7$ vs Na^+/Na measured in different voltage ranges 0.9–3.0 V (solid red), 0.5–3.0 V (blue dots), 0.05–2.2 V (dashed green) and for $\text{Na}_2\text{Ti}_3\text{O}_7$ at 0.05–1.6 V (black thick solid line) (b,c) dQ/dV for the first (b) and second (c) cycles respectively in the same voltage ranges.

Figure 6b and Figure 6c show the derivative of the charge vs voltage (dQ/dV) for the first and second cycle respectively for the three different voltage ranges. It can be seen that when $\text{H}_2\text{Ti}_3\text{O}_7$ is cycled below 0.9 V the process is less reversible as the main reduction and oxidation peaks that appear in the first cycle disappear in the second. Only when the voltage is kept above 0.9 V, the redox peaks of the dQ/dV curve (a broad peak from OCV to 1.4 V and a sharp one at 1.3V) remain in the subsequent cycle, although with a decrease in the amount of charge. Other reactions can be also observed at low voltages, probably due to the insertion of Na ion in carbon¹¹ and the formation of a SEI layer from electrolyte decomposition.

Given the importance of the election of electrolyte in the electrochemical performance²⁵ an initial screening was made concluding that for $\text{H}_2\text{Ti}_3\text{O}_7$, NaClO_4 1M in EC:DMC yielded better performance than by using NaPF_6 as a salt, PC as solvent or FEC as additive. Therefore, the range for the most stable cycling of $\text{H}_2\text{Ti}_3\text{O}_7$ vs. Na^+/Na is 0.9–2.2 V with a reversible capacity of 56 mAh/g in the first cycle corresponding to approximately 0.5 $\text{Na}^+/\text{f.u.}$, which however also drops upon cycling (Figure S3). Despite the observed voltage for sodium insertion is not as low as that of $\text{Na}_2\text{Ti}_3\text{O}_7$, this operating voltage could avoid electrolyte decomposition and SEI layer formation that usually occurs approximately below 1 V, although at 1.4–1.6 V some irreversibility is already observed.

Structural evolution during cycling. In order to understand the irreversibility found in $\text{H}_2\text{Ti}_3\text{O}_7$, the mechanism of sodium insertion was further studied. For this purpose we collected in-situ X-ray diffraction data during the first discharge (Figure 7) and then several datasets after further charge and discharge.

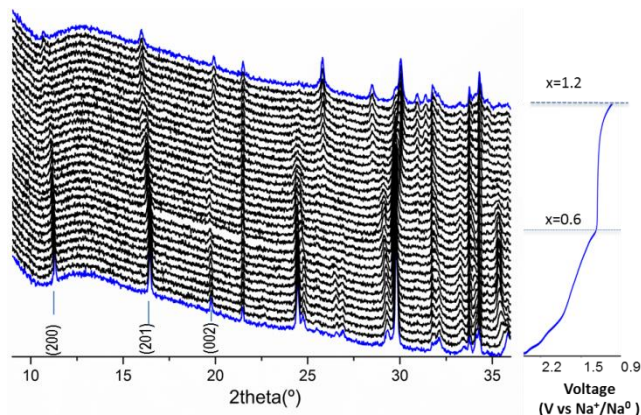


Figure 7. Evolution of XRD patterns collected in-situ during the first discharge cycle of $\text{H}_2\text{Ti}_3\text{O}_7$ powder with carbon Super C65 (65% / 35%) vs Na^+/Na at a current rate of C/50 in the voltage range OCV–0.9V, with the corresponding voltage profile on the right.

During the first reduction (Figure 7) there are no new peaks appearing in the diffraction patterns at the beginning of sodium insertion. Only slight shifts of some reflections such as (200) or (002) towards lower two theta angles occur until the insertion of 0.6 mol of sodium is completed. This indicates a topotactic sodium insertion with formation of the solid solution $\text{H}_2\text{Na}_x\text{Ti}_3\text{O}_7$ that maintains the $\text{H}_2\text{Ti}_3\text{O}_7$ structure type ($C2/m$). The reflection that suffers the major displacement at the initial stage of reduction appears above 35° and corresponds to the (602) reflection, which changes from a d value of 2.486 Å to 2.547 Å. In fact the major changes for this reflection occur at the very early stages of sodium insertion, which agrees with the first of several processes of solid solution occurring until $x=0.6$ sodium ions have been inserted as it can be seen in the non-monotonous change of lattice parameters (Figure S6) and in the appearance of several signals in the dq/dV plot (Figure 6c). This lattice plane corresponds to a diagonal between the $[\text{Ti}_3\text{O}_7]^{2-}$ layers and contains the edge sharing oxygen atoms as well as the middle proton (H1) and most likely the inserted sodium ions as well (see Figure S4). After 0.6 $\text{Na}^+/\text{f.u.}$ are inserted, new reflections appear and start growing in intensity while the previous ones diminish in intensity and vanish. The insertion of 0.6 to 1.0 mol of sodium occurs by a two-phase reaction mechanism in agreement with the plateau observed in the galvanostatic discharge. The new phase appearing in the PXRD pattern is indexed with a different space group ($P2_1/m$ instead of $C2/m$ of the parent material) corresponding to a $\text{Na}_2\text{Ti}_3\text{O}_7$ type unit cell. However, refinement of the atomic positions is not possible given the resolution of the in-situ diffraction data. It nevertheless seems that Na^+ and H^+ ions coexist in the interlayer spacing of the $\text{H}_2\text{Ti}_3\text{O}_7$ type structure up to a limiting amount of sodium. Beyond this amount, the extra sodium cannot be inserted in the interlayer space and a gliding of the layers occurs, opposite to that produced during the ionic exchange from $\text{Na}_2\text{Ti}_3\text{O}_7$ to $\text{H}_2\text{Ti}_3\text{O}_7$. Comparison of the unit cell parameters of the material reduced down to 0.9 V with those of $\text{Na}_2\text{Ti}_3\text{O}_7$ (Figure S6) suggests that the formed phase still contains H^+ from $\text{H}_2\text{Ti}_3\text{O}_7$ as J. Akimoto et al.¹⁷ observed when cycling versus lithium, and which will be confirmed below by ^1H -ssNMR.

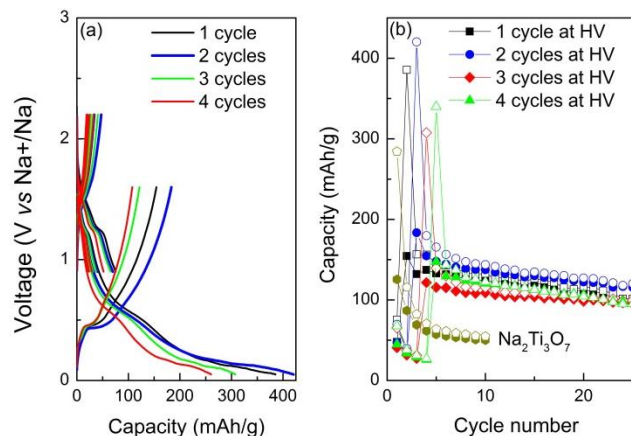


Figure 8. Electrochemical behaviour of $\text{H}_2\text{Ti}_3\text{O}_7$ conditioning for 1-4 cycles at 0.9-2.2 V and then going down to 0.005-1.6 V. (a) Voltage profiles until first cycle at low voltage (b) Capacity vs cycle number in comparison to pristine $\text{Na}_2\text{Ti}_3\text{O}_7$.

Moreover, while sodium ions are inserted in the new phase there is an additional shift of the new reflections in the PXRD patterns, which indicates that a mechanism of solid solution coexists with the two phase reaction. This fact has been also observed for other sodium based systems²⁶ and is assigned to the large lattice mismatch between the sodiated and desodiated phases. Upon charge from 0.9 V up to 2.2 V apparently 0.6 Na/f.u are extracted, but no major change is observed in the powder X-ray diffraction patterns. (Fig S5) Comparison of the pattern collected at the beginning and at the end of charge (Fig S5) hardly shows any difference. This could be assigned to the extraction of H^+ instead of Na^+ with a minor impact on the unit cell parameters as well as in the intensities of the X-ray diffraction peaks. Therefore, and contrary to what happens in $\text{H}_2\text{Ti}_6\text{O}_{13}$ where the two first lithiums replace the protons with chemical reduction of the H^+ into H_2 (which evolves as a gas)²⁷, in $\text{H}_2\text{Ti}_3\text{O}_7$ the protons seem to remain in the structure during reduction and are mainly extracted upon oxidation.

The big irreversible capacity observed in Figure 6 is then due to the irreversible structural changes from $\text{H}_2\text{Ti}_3\text{O}_7$ to $\text{Na}_2\text{Ti}_3\text{O}_7$, and therefore it is very difficult to be improved by carbon coating or using other binder. However as the material cycled vs sodium resembles $\text{Na}_2\text{Ti}_3\text{O}_7$, electrochemical testing at lower voltages after initial high voltage cycling seemed a good alternative and it was carried out. Figure 8a shows the galvanostatic cycling of the material under the following protocol: the material was initially discharged and charged in the voltage range 0.9-2.2 V a different number of times and later continued cycling in the lower voltage range of 0.005-1.6 V. (Figure 8a) As in the case of $\text{Na}_2\text{Ti}_3\text{O}_7$ a large irreversible contribution from the SEI layer appeared below 0.9 V, and a reversible capacity of 100-180 mAh/g, close to that of $\text{Na}_2\text{Ti}_3\text{O}_7$, was obtained for the next cycle. The optimization of the number of cycles at high voltage shows that cycling twice before going to low voltage results in the highest and most stable capacity, 182 mAh/g (Figure 8b). A rate capability test was done in order to see how the kinetics impact the change of capacity and coulombic efficiency exhibited at different C-Rates (C/10, C/5, C/2, C) (Figure 9). There is a loss of capacity at higher C-Rates due to the increase of the polarization. However the capacity retention of this anode material is higher than that of similarly treated pristine $\text{Na}_2\text{Ti}_3\text{O}_7$ ¹¹ which implies

that control over the starting material stoichiometry or microstructure may allow achieving more stable electrodes.

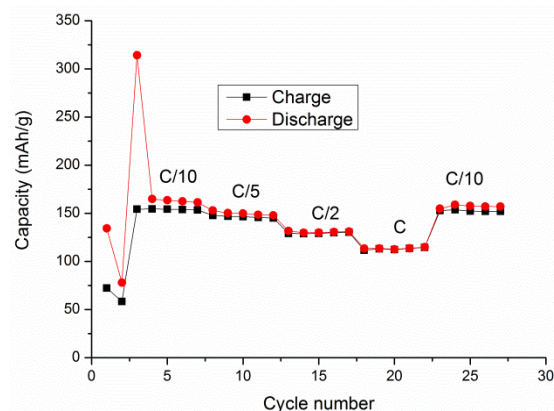


Figure 9. Rate capability of $\text{H}_2\text{Ti}_3\text{O}_7$ conditioning for 2 cycles at 0.9-2.2 V and then going down to 0.005-1.6 V. The first two cycles were done at C/10 and different C-Rates were tested from C/10 to C in the range of 0.005-1.6 V.

Based on the capacity and mean average voltage of the titanate, 127 mAh/g and at 0.75 Volts vs Na^+/Na , in the 4th cycle (that is the first one which there is not SEI layer contribution) and the theoretical values of NaFePO_4 , 154mAh/g of capacity at 2.9 Volts vs Na^+/Na ,^{3, 28} a specific energy density of 175Wh/Kg is obtained, ignoring SEI contribution for the full cell.

In order to see if there are any H^+ remaining after two cycles in the 0.9-2.2 V range, ex-situ MAS ^1H -NMR analysis was done. The integration of the peak at 11 ppm indicates that more than 0.2 $\text{H}^+/\text{f.u}$ of the H1 type remain in the structure (Figure S7) while all H2 and H3 protons forming the “water molecule” have been withdrawn as there is no remaining signal at 13 ppm. On the other hand a new broad proton signal centred at 3.7 ppm appears which corresponds with the signal of the residual electrolyte, EC and DMC.

4. Conclusions

$\text{H}_2\text{Ti}_3\text{O}_7$ was successfully prepared by ionic exchange of $\text{Na}_2\text{Ti}_3\text{O}_7$ in acidic medium. Solid state ^{23}Na -NMR confirmed that the prepared $\text{H}_2\text{Ti}_3\text{O}_7$ contains less than 1% of sodium ions in the structure. Three different types of hydrogen ions were identified and neutron diffraction was used to locate them in the structure. They form hydrogen bonds between adjacent $[\text{Ti}_3\text{O}_7]^{2-}$ layers which we believe are driving the change from a primitive to C-centered unit cell upon ionic exchange. Two of the protons, H2 and H3, are linked to the oxygen that bonds to one titanium atom only, O4. Both of these protons give a single MAS ^1H -ssNMR peak with 75% of the total integrated area. The electrochemical sodium insertion in $\text{H}_2\text{Ti}_3\text{O}_7$ starts with the insertion of 0.6 $\text{Na}^+/\text{f.u}$ through a solid solution mechanism at voltages above 1.3 V vs Na^+/Na . A plateau at 1.3 V indicates that a two phase reaction occurs until 1.2 Na^+ are inserted. The phase formed is similar to $\text{Na}_2\text{Ti}_3\text{O}_7$ as detected by *in-situ* XRD. The delivered capacity and cycling stability in the 0.05-1.6 V range is optimal if the material is previously cycled twice in the 0.9 to 2.2 V range. At this point, at least 0.2 $\text{H}^+/\text{f.u}$ remain in the structure according to ex-situ MAS ^1H -NMR.

5. Acknowledgements

The authors would like to thank Ines Puente Orench, from D1B for her assistance with neutron diffraction experiments, Egoitz Martin for his technical support with XRD, and Michel Armand and Juan Miguel Lopez Del Amo for fruitful discussions. AEB thanks UPV for a FPI-UPV PhD Fellowship. Financial support through project Etortek 10 CIC Energigune, MAT2013-41128-R, and ENE2013-44330-R is acknowledged. The CRG of the D1B and Spins is also acknowledged for providing beam time at ILL and financial support for the neutron experiment.

6. Notes and references

^a CIC Energigune, C/Albert Einstein 48, 01510, Parque Tecnológico de Álava, Miñano, Spain.

^b Departamento de Química Inorgánica, Universidad del País Vasco, UPV/EHU, Bilbao, Spain.

† Electronic Supplementary Information (ESI) available: Plots of Rietveld refinement for XRD and neutron $\lambda=1.287\text{\AA}$ from the combined refinement of all three patterns as well as tables listing the agreement factors and the atomic positions obtained from the combined refinement, Detail of the structure of $\text{H}_2\text{Ti}_3\text{O}_7$ with the 602 plane, Selected XRD patterns of charge during, Fitting of $^1\text{H-NMR}$ of cycled electrode, table with agreement. See DOI: 10.1039/b000000x/

1 Citations here in the format A. Name, B. Name and C. Name, *Journal Title*, 2000, **35**, 3523; A. Name, B. Name and C. Name, *Journal Title*, 2000, **35**, 3523.

¹ Tarascon, J.M.; Armand, M. *Nature*, 2001, **414**, 359.

² V. Palomares, P. Serras, I. Villaluenga, K. Hueso, J. Carretero-Gonzalez, T. Rojo, *Energy Environ. Sci.*, 2012, **5**, 5884.

³ V. Palomares, M. Casas-Cabanas, E. Castillo-Martinez, M. Han, T. Rojo, *Energy and Environ. Sci.*, 2013, **6**, 2312.

⁴ Y. Kim, Y. Park, A. Choi, N.-S. Choi, J. Kim, J. Lee, J. H. Ryu, S. M. Oh, K. T. Lee; *Adv. Mater.*, 2013, **25**, 3045.

⁵ J. Qian, X. Wu, Y. Cao, X. Ai, H. Yang, *Angew. Chem. Int. Ed.* 2013, **52**, 4633.

⁶ S. Komaba, Y. Matsuura, T. Ishikawa, N. Yabuuchi, W. Murata, S. Kuze *Electrochem. Commun.* 2012, **21**, 65.

⁷ A. Darwiche, C. Marino, M. T. Sougrati, B. Fraisse, L. Stievano, and L. Monconduit *J. Am. Chem. Soc.* 2012, **134**, 20805.

⁸ L. Zhao, J. M. Zhao, Y. -S. Hu, H. Li, Z. B. Zhou, M. Armand and L. Q. Chen, *Adv. Energy Mater.*, 2012, **2**, 962.

⁹ E. Castillo-Martinez, J. Carretero-Gonzalez, M. Armand, *Angew. Chem. Int. Ed.* 2014, **126**, 5445.

¹⁰ J. Zhao, L. Zhao, K. Chihara, S. Okada, J.i. Yamaki, S. Matsumoto, S. Kuze, K. Nakane, *J. Power Sources*, 2013, **244**, 752.

¹¹ P. Senguttuvan, G. Rousse, V. Seznec, J. M. Tarascon, M. R. Palacín *Chem. Mater.*, 2011, **23**, 4109.

¹² S. Anderson, A.D. Wadsley, *Acta Crystallogr.*, 1961, **14**, 1245.

¹³ A. Rudola, K. Saravana, C.W. Mason, P. Balaya *J. Mat. Chem A*, 2013, **1**, 2653.

¹⁴ J. Xu, C. Ma, M. Balasubramanianb and Y. S. Meng, *Chem. Comm.*, 2014, **50**, 12564

¹⁵ K. Chiba, N. Kijima, Y. Takahashi, Y. Idemoto, J. Akimoto *Solid State Ionics*, 2008, **178**, 1725.

¹⁶ H. Izawa, S. Kikkawa, M. Koizumi, *J. Phys. Chem.* 1982, **86**, 5023.

¹⁷ J. Akimoto, K. Chiba, N. Kijima, H. Hayakawa, S. Hayashi, Y. Gotoh, Y. Idemoto, *J. Echem. Soc.* 2011, **158**, A546.

¹⁸ T. P. Feist, P. K. Davies, *J. Solid State Chem.* 1992, **101**, 275.

¹⁹ K. Kataoka, N. Kijima, and J. Akimoto, *Inorg. Chem.*, 2013, **52**, 13861

²⁰ J. Rodriguez-Carvajal, *Physica B.*, 1993, **192**, 55.

²¹ D. Massiot, F. Fayon, M. Capron, I. King, S. Le Calvé, B. Alonso, J. O. Durand, B. Bujoli, Z. Gan and G. Hoatson, *Magnetic Resonance in Chemistry*, 2002, **40**, 70-76.

²² A. Orera, M. T. Azcondo, F. Garcia-Alvarado, J. Sanz, I. Sobrados, J. Rodriguez-Carvajal, U. Amador, *Inorg. Chem.* 2009, **48**, 7659.

²³ J. C. Pérez-Flores, F. García-Alvarado, M. Hoelzel, I. Sobrados, J. Sanz, A. Kuhn, *Dalton Trans.*, 2012, 41, 14633

²⁴ Y. Wang, X. Yu, S. Xu, J. Bai, R. Xiao, Y.-S. Hu, H. Li, X.-Q. Yang, L. Chen, X. Huang, *Nat. Commun.*, 2013 **4**, 2365.

²⁵ S. Komaba, W. Murata, T. Ishikawa, N. Yabuuchi, T. Ozeki, T. Nakayama, A. Ogata, K. Gotoh, and K. Fujiwara, *Adv. Funct. Mater.*, 2011, **21**, 3859

²⁶ M. Galceran, D. Saurel, B. Acebedo, V. V. Roddatis, E. Martin, T. Rojo and M. Casas-Cabanas, *Phys. Chem. Chem. Phys.*, 2014, **16**, 8837.

²⁷ J. C. Perez-Flores, C. Baetz, M. Hoelzel, A. Kuhn and F. Garcia-Alvarado, *RSC Advances*, 2012, **2**, 3530.

²⁸ S. M. Oh, S. T. Myung, J. Hassoun, B. Scrosati, Y. K. Sun, *Electrochem. Commun.* 2012, **22**, 149